

Crossed Andreev effects in two-dimensional quantum Hall systems

Zhe Hou,¹ Yanxia Xing,² Ai-Min Guo,³ and Qing-Feng Sun^{1,4,*}

¹*International Center for Quantum Materials, School of Physics, Peking University, Beijing 100871, China*

²*Department of Physics, Beijing Institute of Technology, Beijing 100081, China*

³*Department of Physics, Harbin Institute of Technology, Harbin 150001, China*

⁴*Collaborative Innovation Center of Quantum Matter, Beijing 100871, China*

(Received 11 April 2016; revised manuscript received 13 July 2016; published 22 August 2016)

We study the crossed Andreev effects in two-dimensional conductor/superconductor hybrid systems under a perpendicular magnetic field. Both a graphene/superconductor hybrid system and an electron gas/superconductor one are considered. It is shown that an exclusive crossed Andreev reflection, with other Andreev reflections being completely suppressed, is obtained in a high magnetic field because of the chiral edge states in the quantum Hall regime. Importantly, the exclusive crossed Andreev reflection not only holds for a wide range of system parameters, e.g., the size of system, the width of central superconductor, and the quality of coupling between the graphene and the superconductor, but also is very robust against disorder. When the applied bias is within the superconductor gap, a robust Cooper-pair splitting process with high-efficiency can be realized in this system.

DOI: [10.1103/PhysRevB.94.064516](https://doi.org/10.1103/PhysRevB.94.064516)

I. INTRODUCTION

The Cooper pairs in a superconductor can be used as a natural source of nonlocal Einstein-Podolsky-Rosen (EPR) electron pairs [1,2]. By splitting the electrons in a Cooper pair, one obtains two spatially separated electrons which still keep their spin and momentum entangled. The Cooper-pair splitting is the inverse process of crossed Andreev reflection (CAR), which has been extensively studied for many years [3–20]. The CAR process occurs at the interface between a normal conductor and the superconductor, where an electron is injected from one terminal of the normal conductor and is then reflected out as a hole at the other terminal, and a Cooper pair forms in the superconductor. Except for the CAR, there also exists local Andreev reflection (LAR), where the hole is reflected into the same terminal. The CAR process usually competes with the LAR one. To split a Cooper pair efficiently, the LAR process has to be suppressed.

Up to now, many proposals have been put forward to realize the splitting of Cooper pairs [3–18] for its promising applications in quantum communication and quantum computing [9,21,22]. For example, some Cooper-pair splitters have been theoretically proposed in the system by coupling a superconductor with quantum dots [9,11,12], carbon nanotubes [13,14], Luttinger liquid wires [15], and graphene [16–18]. On the experimental sides [23–25], the Cooper-pair splitters have been realized in the system by coupling a superconductor with two quantum dots, where a central superconducting finger is connected with two quantum dots and each quantum dot is coupled with a metallic lead. In the Coulomb blockade regime, the electrons in a Cooper pair can tunnel into different leads coherently from the superconductor, and the LAR process can be considerably suppressed by tuning the energy levels of the quantum dots. However, in this Cooper-pair splitter, the LAR process cannot be completely suppressed, and thus the entangled electrons are not spatially separated completely [7]. Furthermore, to improve the efficiency of the

CAR process, the parameters, such as the bias and the gate voltage of the quantum dots, have to be accurate. It may be difficult for experimental implementation of the Cooper-pair splitter.

Recently, due to the emergence of topological insulators and Majorana fermion, some Cooper-pair splitters are proposed based on the hybrid system of the superconductor and the topological insulators or the Majorana fermion [7,26–30]. For example, in a two-dimensional (2D) topological insulator-superconductor-2D topological insulator junction, an all-electric Cooper-pair splitter was proposed by Reinthaler *et al.* [30]. James *et al.* [7] proposed an exclusive CAR device by inducing superconductivity on a AIII class topological insulator wire which supports two topological phases with one or two Majorana fermion end states. In the phase with two Majorana fermions, the LAR is completely suppressed at the normal lead/topological superconductor interface at zero bias, resulting in correlated and spin-polarized currents in the leads.

However, all of the previous Cooper-pair splitters have several disadvantages. Since the incoming electron and the outgoing hole in the CAR process locate in spatially separated terminals, the width L of the central superconductor is required to be less than the superconducting coherent length ξ , and the CAR coefficient would decay quickly to zero when $L > \xi$. Typically, the LAR also occurs inevitably, in which the outgoing hole comes back to the same terminal as the incoming electron. In many Cooper-pair splitters, the LAR is usually much larger than the CAR and the efficiency of the Cooper-pair splitting is quite low. Furthermore, many Cooper-pair splitters are too elaborate to be realized experimentally. They can work only under certain special parameters and are usually not robust against disorders and impurities, which exist inevitably in the experiments. As a result, the CAR process is strongly suppressed and the Cooper-pair splitting efficiency is very low. Here we also notice that very recently, Zhang *et al.* proposed a Cooper-pair splitter based on a quantum anomalous Hall insulator (QAHI) [31]. Due to the unidirectionality of the chiral edge states in the QAHI, the LAR can be suppressed completely and only the CAR occurs

*sunqf@pku.edu.cn

in the QAHI-superconductor-QAHI junction. Consequently, this QAHI-based Cooper-pair splitter can be very efficient and be robust against the disorders and can work even if the size of the superconductor electrode is much larger than the superconducting coherent length. However, it is very difficult to fabricate the QAHI in the experiment, although the QAHI has been successfully realized in the magnetic topological insulator with the temperature being at the order of mK [32,33]. Therefore, it is an urgent task to propose a Cooper-pair splitter which is of high efficiency and is robust against the disorder and works in large-superconductor size.

Graphene is a 2D material with a unique band structure [34,35]. Electrons in graphene exhibit relativistic-like behavior near the Dirac point. One of the peculiar properties of graphene is the half integer quantum Hall effect with the chiral edge states. In this paper, we investigate the electron transport through a three-terminal graphene/superconductor system and propose a robust Cooper-pair splitter with the aid of the chiral edge states in the quantum Hall system. In general, the quantum Hall effect and the superconductivity are mutually exclusive because the former phenomenon exists in the presence of strong magnetic field, whereas the latter one will be destroyed by the strong magnetic field. However, with modern progress in materials science, the quantum Hall effect can be observed at a much smaller magnetic field, which ensures the possibility of coexistence of the quantum Hall effect and the superconductivity [36–40]. For example, both the quantum Hall effect and the superconductivity have been successfully realized in the junction which consists of the 2D electron gas and the Nb compounds, where the 2D electron gas with high mobility possesses the quantum Hall regime under sufficiently small magnetic field and the Nb compounds have a high critical magnetic field [38]. The coexistence of the quantum Hall effect and the superconductivity has also been observed in the graphene/superconductor hybrid system [39].

By using the tight-binding model and the nonequilibrium Green’s function method, we obtain expressions of Andreev reflection coefficients and normal transmission coefficients under different magnetic fields. In strong magnetic field, the chiral edge states form in the graphene, and the electrons (holes) can be reflected unidirectionally as the holes (electrons) at the interface between the graphene and the superconductor. Because of the unidirectionality of the chiral edge states, the outgoing hole will be transmitted to the other graphene terminal and only the CAR occurs, as shown in Fig. 1(a).

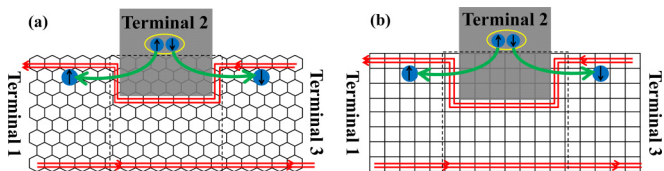


FIG. 1. Schematic diagram for three-terminal hybrid system of (a) graphene/superconductor and (b) two-dimensional electron gas/superconductor. The red lines denote the edge states due to the strong magnetic field B . With the aid of the unidirectional chiral edge states, the Cooper pairs in the superconductor lead can be split into two separated terminals.

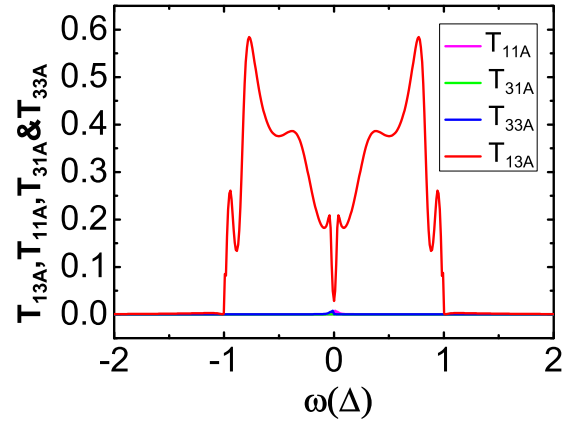


FIG. 2. Andreev reflection coefficients T_A versus incident energy ω for the graphene/superconductor hybrid system at $\phi = 0.003$. Due to the chiral edge states, the exclusive CAR coefficient T_{13A} is very large, with the other Andreev reflection coefficients being prohibited. The parameters are listed as follows: the Dirac point energy $E_0 = -5\Delta$, the width of the graphene nanoribbon $N = 50$, the length of the central region $L = 30$, the size of the covered area of the superconductor $M = 15$, the coupling strength between the graphene and the superconductor $t_c = t$, and the disorder strength $W = 0$.

Notice that the LAR happens only if the outgoing hole is scattered from one edge of the graphene to the other edge. In the quantum Hall regime, the scattering between the two edges is almost impossible, and hence the LAR is completely inhibited and an exclusive CAR emerges. Figure 2 shows the main results in this paper, where only the CAR coefficient T_{13A} has large value and the other Andreev reflection coefficients are almost zero. As a result, this device can serve as a robust Cooper-pair splitter with high efficiency. This Cooper-pair splitter can be very robust against the disorder. As long as the chiral edge states are present, the Cooper-pair splitter can work well. Furthermore, it works well even when the width L of the superconductor is larger than the superconducting coherent length ξ and the width L breaks through the size limitation of previous Cooper-pair splitters. In addition, the exclusive CAR process, with the LAR being completely suppressed, can hold for a wide range of system parameters, such as the width of the graphene nanoribbon, the coupling between the superconductor, and the graphene. Finally, a 2D electron gas is considered instead of the graphene and similar results are obtained due to the emergence of the chiral edge states, which are induced by external magnetic field [see Fig. 1 (b)].

The rest of the paper is constructed as follows. In Sec. II, the theoretical model is presented and the expressions of the normal transmission coefficients and the Andreev reflection coefficients are derived. In Sec. III, we numerically investigate the transmission coefficient, the CAR coefficient, and the LAR coefficient and discuss the characteristics of the proposed Cooper-pair splitter in the graphene/superconductor hybrid system. In Sec. IV, we change the Dirac point of the graphene to demonstrate the regime of the CAR and the LAR. Finally, the results are summarized in Sec. V. The Cooper-pair splitter in the 2D electron gas/superconductor hybrid system is presented in the Appendix.

II. MODEL AND FORMULISM

We consider a three-terminal system by coupling a zigzag edged graphene nanoribbon with a superconductor lead [as shown in Fig. 1(a)]. The central region with width N and length L , as labeled by the rectangular area in Fig. 1(a), is partly covered by the superconductor lead. The covered region is described by width M and length L with $2M(2L - 1)$ carbon atoms. In Fig. 1(a), it shows a system with $N = 5$, $L = 7$, and $M = 2$.

The Hamiltonian of the system is

$$H = H_G + H_S + H_C, \quad (1)$$

where H_G , H_S , and H_C are the Hamiltonians of the graphene nanoribbon, the superconductor lead, and the coupling between them, respectively. In the tight-binding representation, H_G is [41,42]

$$H_G = \sum_{i,\sigma} E_i a_{i\sigma}^\dagger a_{i\sigma} - \sum_{(ij),\sigma} t e^{i\phi_{ij}} a_{i\sigma}^\dagger a_{j\sigma}, \quad (2)$$

where $a_{i\sigma}^\dagger$ and $a_{i\sigma}$ are the creation and annihilation operators at the discrete site i , and $E_i = E_0 + \omega_i$ denotes the on-site energy. E_0 is the Dirac point energy which can be controlled experimentally by gate voltage and ω_i is the on-site disordered energy. In the experiment, disorder and impurity exist inevitably. The disorder in graphene p - n junction can result in several extra conductance plateaus [42–44]. Furthermore, the charge puddle disorder has been confirmed in the graphene by recent experiments [45,46]. Here we consider that the disorder exists only in the central scattering region. $\omega_i = 0$ at the left and right graphene terminals, while for the central region, ω_i is uniformly distributed in the range $[-W/2, W/2]$, with W being the disorder strength. The second term in H_G describes the nearest-neighbor hopping. Because of a uniform perpendicular magnetic field on the graphene nanoribbon, a phase ϕ_{ij} is added in the hopping element and $\phi_{ij} = \int_i^j \vec{A} \cdot d\vec{l} / \phi_0$ with the vector potential $\vec{A} = (-By, 0, 0)$ and $\phi_0 = \hbar/e$. Note that in the superconductor lead and the covered graphene region, no magnetic field exists due to the Meissner effect and $\phi_{ij} = 0$ in these regions.

As for the superconductor lead, we consider the BCS Hamiltonian and H_S is

$$H_S = \sum_{\mathbf{k},\sigma} \epsilon_{\mathbf{k}} b_{\mathbf{k}\sigma}^\dagger b_{\mathbf{k}\sigma} + \sum_{\mathbf{k}} (\Delta b_{\mathbf{k}\uparrow}^\dagger b_{-\mathbf{k}\downarrow}^\dagger + \Delta b_{-\mathbf{k}\downarrow} b_{\mathbf{k}\uparrow}), \quad (3)$$

where Δ is the superconductor gap and $b_{\mathbf{k}\sigma}^\dagger$ ($b_{\mathbf{k}\sigma}$) is the creation (annihilation) operator in the superconductor lead with momentum $\mathbf{k} = (k_x, k_y)$. The coupling between the superconductor and the graphene is described by the Hamiltonian

$$H_C = \sum_{i,\sigma} t_c a_{i\sigma}^\dagger b_{i\sigma} + \text{H.c.}, \quad (4)$$

where $b_{i\sigma}$ is the annihilation operator at site i and $b_{i\sigma} = \sum_{\mathbf{k}} e^{i\mathbf{k}\cdot\mathbf{r}_i} b_{\mathbf{k}\sigma}$. Here \mathbf{r}_i is the position of the i th carbon atom in real space and t_c is the coupling parameter between the superconductor and the graphene.

By using the nonequilibrium Green's function method, we can obtain the normal transmission coefficient $T_{nm(m \neq n)N}$, the

CAR coefficient $T_{nm(m \neq n)A}$, and the LAR coefficient $T_{nm(m=n)A}$ between the graphene terminals $m = 1, 3$ and $n = 1, 3$ [47–49],

$$T_{nm(m \neq n)N}^\sigma(\omega) = \text{Tr}[\mathbf{G}^r \Gamma_{n,\sigma} \mathbf{G}^a \Gamma_{m,\sigma}], \quad (5)$$

$$T_{nmA}^\sigma(\omega) = \text{Tr}[\mathbf{G}^r \Gamma_{n,\bar{\sigma}} \mathbf{G}^a \Gamma_{m,\sigma}], \quad (6)$$

where σ represents spin-up electron (\uparrow) and spin-down hole (\downarrow) in the 2×2 Nambu space and $\bar{\sigma} = \uparrow$ (\downarrow) for $\sigma = \downarrow$ (\uparrow). Since the Pauli matrices $\sigma_{x,y,z}$ are commutative with the Hamiltonian H , the transmission coefficient and the Andreev reflection one satisfy $T_{nmN}^\uparrow = T_{nmN}^\downarrow$ and $T_{nmA}^\uparrow = T_{nmA}^\downarrow$, and we ignore the superscript “ $\sigma = \uparrow, \downarrow$ ” in the following for representation simplicity. T_{13N} (T_{31N}) represents normal tunneling possibility from terminal 3 (terminal 1) to terminal 1 (terminal 3). The LAR coefficient T_{nmA} (CAR coefficient $T_{nm(m \neq n)A}$) is the probability of an electron coming from the graphene terminal- m and getting Andreev reflected as a hole into the same terminal- m (different terminal- n). The linewidth function $\Gamma_n(\omega) \equiv i[\Sigma_n^\uparrow - (\Sigma_n^\uparrow)^\dagger]$ and $\Sigma_n^r(\omega)$ is the retarded self-energy due to the coupling between the central region and the terminal n . $\mathbf{G}^{r(a)}(\omega)$ is the retarded (advanced) Green's function of the central region in the Nambu space, and $\mathbf{G}^r(\omega) = [\mathbf{G}^a(\omega)]^\dagger = [\omega \mathbf{I} - \mathbf{H}_C - \sum_{n=1,2,3} \Sigma_n^r(\omega)]^{-1}$, with \mathbf{H}_C being the Hamiltonian matrix for the central region. For the self-energies $\Sigma_{1(3)}^r(\omega)$ of the left and right leads, we have $\Sigma_{1(3),ij}^r(\omega) = t \mathbf{g}_{1(3),ij}^r(\omega) t$, where $\mathbf{g}_{1(3),ij}^r(\omega)$ is the surface Green's function of terminal 1 (terminal 3), which can be numerically calculated [50]. For the self-energy of the superconductor terminal, we have $\Sigma_{2,ij}^r(\omega) = t_c \mathbf{g}_{2,ij}^r(\omega) t_c$ and $\mathbf{g}_{2,ij}^r(\omega)$ is [47]

$$\mathbf{g}_{2,ij}^r(\omega) = -i\pi\rho\beta(\omega)J_0(k_F|\mathbf{r}_i - \mathbf{r}_j|) \otimes \begin{pmatrix} 1 & \Delta/\omega \\ \Delta/\omega & 1 \end{pmatrix}, \quad (7)$$

where ρ represents normal density of states for the superconductor and $J_0(k_F|\mathbf{r}_i - \mathbf{r}_j|)$ is the 0th-order Bessel function, with k_F being the Fermi wave vector. $\beta(\omega) = -i\omega/\sqrt{\Delta^2 - \omega^2}$ for $|\omega| < \Delta$ and $\beta(\omega) = |\omega|/\sqrt{\omega^2 - \Delta^2}$ for $|\omega| > \Delta$ [47–49]. For simplicity, we assume that $J_0(k_F|\mathbf{r}_i - \mathbf{r}_j|) = 1$ for $i = j$ and otherwise $J_0(k_F|\mathbf{r}_i - \mathbf{r}_j|) = 0$ for $i \neq j$. This assumption is reasonable because k_F is usually in the order of \AA^{-1} . After this assumption, the superconductor lead seems to be made up of one-dimensional wires and each carbon atom in the central region connects independently with a superconductor, which has been assumed in Ref. [51]. Then Eq.(7) can be reduced as

$$\mathbf{g}_{2,ij}^r(\omega) = -i\pi\rho\beta(\omega)\delta_{ij} \otimes \begin{pmatrix} 1 & \Delta/\omega \\ \Delta/\omega & 1 \end{pmatrix}. \quad (8)$$

By employing these transmission coefficients, the current flowing from terminal 3 into the central region can be obtained straightforwardly [47,52]:

$$I_3 = \frac{2e}{h} \int d\omega \{ T_{23N}(f_{3+} - f_2) + T_{13N}(f_{3+} - f_{1+}) + T_{13A}(f_{3+} - f_{1-}) + T_{33A}(f_{3+} - f_{3-}) \}. \quad (9)$$

Here $f_{\alpha\pm}(\omega) = 1/\{\exp[(\omega \mp eV_\alpha)/k_B T] + 1\}$ is the Fermi distribution function for the terminal α , with the temperature T and the bias V_α . The bias of the superconductor lead V_2 is set to zero.

In the following numerical calculations, we set the hopping energy $t = 2.75$ eV, the nearest-neighbor carbon-carbon distance $a = 0.142$ nm, and the superconductor gap $\Delta = 1$ meV. The magnetic field B is expressed in terms of $\phi \equiv (3\sqrt{3}/4)a^2 B/\phi_0$ and $(3\sqrt{3}/2)a^2 B$ is the magnetic flux in the honeycomb lattice. In the presence of disorder, the curves are averaged over 500 random configurations.

III. THREE-TERMINAL GRAPHENE/SUPERCONDUCTOR HYBRID SYSTEM

We first study the electron transport properties of the graphene/superconductor hybrid system under different magnetic fields. Figure 3 shows the Andreev reflection coefficients T_A and the normal transmission coefficients T_N versus the energy ω of the incident electron. In the absence of a magnetic field ($\phi = 0$) or for a weak magnetic field ($\phi = 0.0005$ and 0.001), both the LAR process and the CAR one can occur for the incident electron from terminal 1 or from terminal 3 [see Figs. 3(a)–3(d)]. The LAR coefficients T_{11A} and T_{33A} can be quite large, and the CAR coefficients T_{31A} and T_{13A} are relatively small when the energy ω is within the superconductor gap, i.e., $|\omega| < \Delta$. Both the LAR and the CAR coefficients decay quickly when ω is beyond the superconductor gap, which is similar to usual normal-superconductor junction [53]. The normal transmission coefficients T_{13N} and T_{31N} are large when $|\omega| < \Delta$ and are decreased when $|\omega| > \Delta$, because the tunneling from the graphene to the superconductor can happen when $|\omega| > \Delta$. When the magnetic field is gradually increased to $\phi = 0.003$, one notices the following features. (i) For the incident electron from terminal 1, the Andreev reflection coefficients T_{11A} and T_{31A} are gradually declined to zero, and the normal transmission coefficient T_{31N} is gradually increased to one [see Figs. 3(a), 3(c), and 3(e)]. This indicates that the electrons tunnel directly from terminal 1 into terminal 3 without being Andreev reflected by the superconductor.

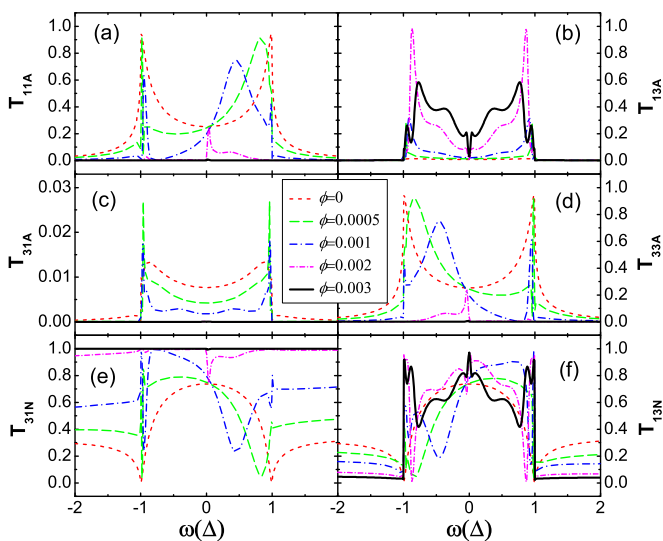


FIG. 3. Andreev reflection coefficients T_A and normal transmission coefficients T_N versus incident energy ω for the graphene/superconductor hybrid system under different magnetic fields ϕ . The other parameters are the same as those of Fig. 2.

(ii) For the incident electron from terminal 3, the LAR coefficient T_{33A} is shrunk to zero and the CAR coefficient T_{13A} is increased to a remarkable value [see Figs. 3(b) and 3(d)], and $T_{13A} + T_{13N} = 1$ when $|\omega| < \Delta$ [see Figs. 3(b) and 3(f)]. This implies that when the electrons encounter the superconductor, they get Andreev reflected and no backscattering occurs. It should be mentioned that the corresponding magnetic field B is about 75 T when $\phi = 0.003$. Since the width of the graphene nanoribbon in Fig. 3 is very narrow [when $N = 50$, the width is about $(3N - 1)a \approx 21$ nm], the magnetic field should be sufficiently strong so that the quantum Hall effect could appear, while for a wide graphene nanoribbon, the magnetic field can be much weaker.

Now we explain the numerical results in Fig. 3. In the weak or zero magnetic field, the wave function of the incident electron can extend over the whole bulk of the graphene nanoribbon. When the electron encounters the superconductor, the Andreev reflections occur at the interface of the graphene and the superconductor and give rise to either the LAR or the CAR. Since the Fermi energy of the superconducting lead is $E_F = 0$, which is far away from the Dirac point $E_0 = -5\Delta$ of the graphene in Fig. 3, the incident electron and the reflected hole locate in the same band [see Fig. 8(c)]. As a result, the Andreev retro-reflection dominates in this situation and the LAR is more pronounced than the CAR [52]. This accounts for the phenomenon that the LAR coefficient is much larger than the CAR one in the weak magnetic field. While in the relatively strong magnetic field (e.g., $\phi = 0.003$), both the Landau levels and the edge states form, as depicted by the red lines in Fig. 1. In this case, the incident electron from terminal 1 transports along the bottom red line of Fig. 1(a) and tunnels directly into terminal 3 without encountering the superconductor. Thus, no backscattering and Andreev reflections occur, and $T_{11A} = T_{31A} = 0$ and $T_{31N} = 1$, which equals the filling factor ν of the Landau levels. On the other hand, the incident electron from terminal 3 transports along the top red line of Fig. 1(a) and will be Andreev reflected at the interface of the graphene and the superconductor. Since the reflected hole lies in the same band as the incident electron mentioned above and their edge states have the same chirality, the reflected hole moves along the same direction of the incident electron. Then only the CAR process occurs and the LAR process is completely suppressed. Additionally, since the normal tunneling from the graphene into the superconductor is prohibited when the energy ω is within the superconductor gap, and the backscattering at the interface is also prohibited due to the chiral edge states, we have $T_{13A} + T_{13N} = 1$ because of current conservation.

Next we study the transport properties of the graphene/superconductor hybrid system in the regime of high magnetic fields. In Fig. 4 we plot the Andreev reflection coefficients T_{nmA} and the normal transmission coefficients T_{13N} versus the incident energy ω for different strong magnetic fields. The T_{11A} , T_{33A} , and T_{31A} are completely suppressed and are almost zero, and only T_{13A} and T_{13N} are remarkable. In addition, $T_{13A} + T_{13N} = 1$ when ω is within the superconductor gap Δ . These are similar to the results of $\phi = 0.003$ in Fig. 3. When the bias of terminal 1 is equal to that of terminal 3, i.e., $V_1 = V_3$, the normal tunneling term T_{13N} does not contribute to the current [see Eq. (9)]. In the case of small bias ($|eV| < \Delta$), the tunneling from the graphene

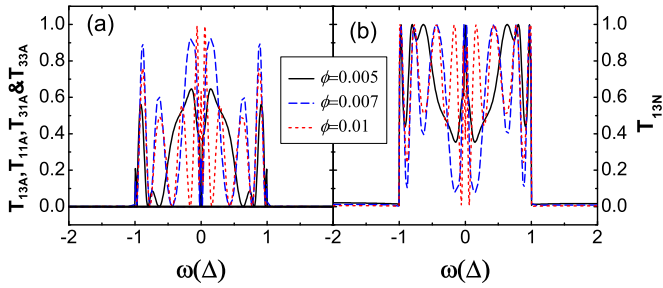


FIG. 4. (a) Andreev reflection coefficients T_A and (b) transmission coefficient T_{13N} versus incident energy ω in the regime of strong magnetic fields ϕ . In panel (a), only T_{13A} has large value; T_{11A} , T_{31A} , and T_{33A} are almost zero, and their curves overlap together and are shown by the black bold lines. The other parameters are the same as those of Fig. 2.

to the superconductor is also prohibited ($T_{23N} = 0$) due to the existence of the superconductor gap. Then the current in Eq. (9) can be reduced to

$$I_3 = (2e/h) \int d\omega \{ T_{13A}(f_{3+} - f_{1-}) + T_{33A}(f_{3+} - f_{3-}) \}, \quad (10)$$

in which only the Andreev reflection contributes to the current. Because $T_{11A} = T_{33A} = 0$ at strong magnetic field, the differential conductance is $G_3 = \frac{dI_3}{dV} = \frac{2e^2}{h} [T_{13A}(eV) + T_{13A}(-eV)]$ at zero temperature. Thus, in the regime of strong magnetic field, an exclusive CAR T_{13A} is obtained, with both the LAR and the normal tunneling being completely prohibited. Notice that since the relation $T_{13A}^\uparrow = T_{13A}^\downarrow$ always holds, and the spin-up and spin-down electrons from a Cooper-pair transport to terminal 1 and terminal 3 randomly, the two spatially separated electrons can keep their spin and momentum entangled. By setting the bias of the superconductor slightly higher than one of the graphene terminals, the current can be driven from the superconductor to the graphene, and the Cooper pair can be split into two separated electrons which will flow into different leads [see Fig. 1(a)]. This generates two spatially separated electron flows with entangled spin and momentum.

Here we emphasize that the efficiency of this Cooper-pair splitter is very high, although the value of the CAR shows oscillation behavior. From Eq. (10), we can define splitting efficiency as

$$\eta = \frac{\int d\omega \{ T_{13A}(f_{3+} - f_{1-}) \}}{\int d\omega \{ T_{13A}(f_{3+} - f_{1-}) + T_{33A}(f_{3+} - f_{3-}) \}}. \quad (11)$$

Here η describes the probability to obtain two spatially separated electrons when a Cooper pair is split. Because the LAR is completely suppressed with $T_{33A} = 0$ in the quantum Hall regime, the splitting efficiency η of a Cooper pair is always 100%.

Now let us study how the exclusive CAR coefficient T_{13A} in the graphene/superconductor system is affected by the system parameters. Figure 5(a) shows T_{13A} versus ω for different length L of the central region. We find that T_{13A} can always reach large value by varying L from 30 to 1000. In addition, T_{13A} oscillates with the energy ω , and the

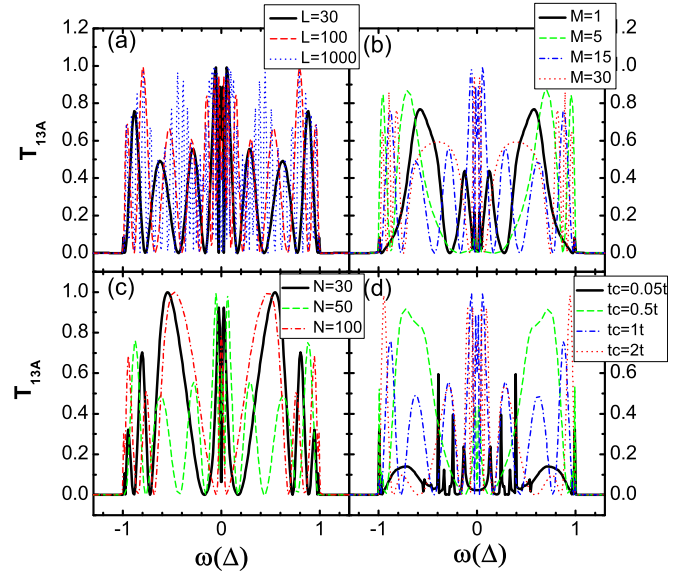


FIG. 5. Energy-dependent CAR coefficient T_{13A} by considering different L (a), M (b), N (c), and t_c (d) in the graphene/superconductor hybrid system. If the parameters are not shown in the legend, they are as follows: $L = 30$, $N = 50$, $M = 15$, $t_c = t$, $E_0 = -5\Delta$, $\phi = 0.01$, and $W = 0$. Here T_{11A} , T_{31A} , and T_{33A} are not shown in the figure because they are all zero.

oscillation frequency is increased by increasing the length L [54,55], because the Fabry-Pérot-like interference occurs in this three-terminal system. In particular, for $L = 1000$, the length of the central region is $\sqrt{3}aL \approx 246$ nm, which is much greater than the superconducting coherent length. However, the CAR coefficient T_{13A} is still very large in this case. As compared with previously proposed Cooper-pair splitters that the length of the central region should be less than the superconductor coherent length ξ , we show in the present study that the CAR process is not confined by the length L because of the unidirectional chiral edge states. The exclusive CAR coefficient T_{13A} can also be quite large by changing the width N of the graphene nanoribbon [as shown in Fig. 5(c)]. In fact, as long as the graphene nanoribbon is wide enough so that the top and bottom chiral edge states do not mix together, an exclusive CAR process can always be obtained. Figures 5(b) and 5(d) show how T_{13A} be affected by the covered area and the coupling strength between the superconductor and the graphene. By varying the width M of the covered area of the superconductor on the graphene and the coupling strength t_c , T_{13A} can still have large value. These results show that the exclusive CAR process in our system can hold very well in a wide range of the system parameters, which is helpful for experimental implementation of the Cooper-pair splitter.

Let us study the effect of the disorder on the exclusive CAR. Here we consider the on-site Anderson disorder which only exists in the central region. Figure 6 shows the Andreev reflection coefficients T_A and the normal transmission coefficient T_N versus the incident energy ω for different disorder strengths W . By increasing the disorder strength W from 1 to 100 meV, the above coefficients are almost unaffected, indicating that our Cooper-pair splitter is very robust. By further increasing W to 1000 meV, the LAR coefficients T_{11A}

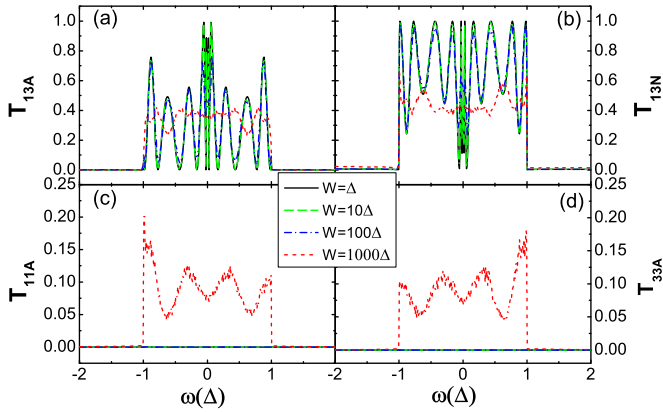


FIG. 6. T_A and T_N versus ω for different disorder strengths W . The parameters are $E_0 = -5\Delta$, $N = 50$, $L = 30$, $M = 15$, $t_c = t$, and $\phi = 0.01$.

and T_{33A} become nonzero, and the oscillation behavior of T_{13A} and T_{13N} disappears. This is due to the fact that the system goes into the diffusive regime at large disorder and the edge states are destroyed by the disorder. Therefore, as long as the edge states survive, the exclusive CAR T_{13A} can persist. This means that the exclusive CAR, i.e., the Cooper-pair splitter, is robust owing to the quantum Hall effect.

In the Appendix, we show the electron transport properties of a three-terminal 2D electron gas/superconductor hybrid system and obtain similar results as the graphene/superconductor hybrid system. Although the two systems have different band structures and electronic behaviors, both of them can work as a robust Cooper-pair splitter, owing to the chiral edge states which are induced by strong magnetic field. However, in general, the graphene/superconductor system has more advantages as compared with the 2D electron gas/superconductor one. This is attributed to the fact that the graphene has a unique band structure with a linear dispersion relation near the Dirac point, and the zeroth Landau level at the Dirac point is well separated from the first Landau level.

IV. GRAPHENE/SUPERCONDUCTOR SYSTEM WITH DIRAC POINT NEAR FERMI ENERGY

Let us change the Dirac point energy E_0 from -5Δ to -0.5Δ to see the interesting behavior of the LAR and the CAR in the graphene/superconductor system. In the experiment, the Dirac point energy can be easily tuned by the gate voltage. At zero magnetic field, the Andreev reflection in the graphene/superconductor interface can be divided into the retroreflection and the specular reflection, according to the situation that the incoming electron and the reflected hole locate in the same bands or different ones [see Figs. 8(b) and 8(c)] [6,52,56]. When the Dirac point is near the Fermi energy, the specular reflection is dominant. While in the presence of the magnetic field, the movement of the reflected hole will be changed and the results are totally different. Figure 7 shows the Andreev reflection coefficients T_A and the normal transmission coefficients T_N versus the incident electron energy ω under different magnetic fields. Similar to the case of $E_0 = -5\Delta$,

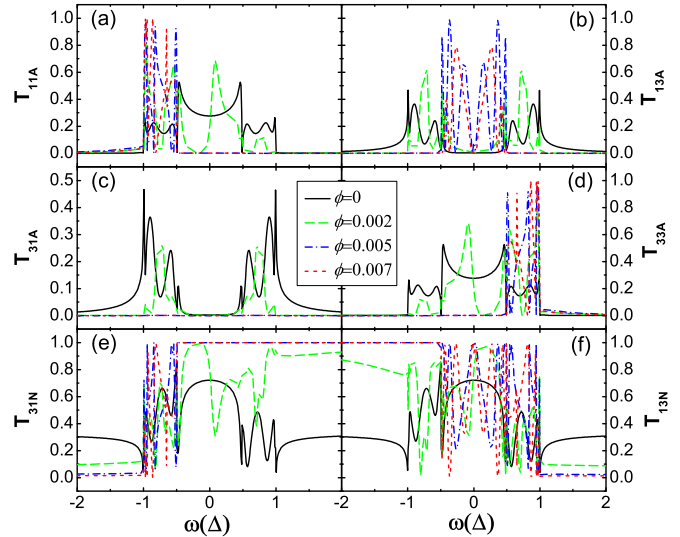


FIG. 7. Andreev reflection coefficients T_A and normal transmission coefficients T_N versus energy ω for the graphene/superconductor hybrid system under different magnetic fields, with the Dirac point energy $E_0 = -0.5\Delta$. The other parameters are $N = 50$, $L = 30$, $M = 15$, $t_c = t$, and $W = 0$.

the edge states gradually form in the three-terminal system by increasing the magnetic field and some unique properties appear. Here we emphasize the following two facts: (i) When $|\omega| > |E_0| = 0.5\Delta$, the incident electron and the reflected hole locate in different bands, i.e., the valence band ($E < E_0$) with negative chirality and the conduction band ($E > E_0$) with positive chirality [see Fig. 8(b)]. Thus, under strong magnetic field, the direction of the unidirectional chiral edge states is opposite for the incident electron and the reflected hole. (ii) When $|\omega| < |E_0|$, the incident electron and the reflected hole locate in the same band [see Fig. 8(c)], and the direction of the chiral edge states is the same.

Now we focus on the case of high magnetic field (e.g., $\phi = 0.007$) in Fig. 7. For the incident electron from terminal 1, the electron transports along the top edge state from left to right when $\omega < E_0 = -0.5\Delta$ [see Fig. 8(a)], then it meets the superconductor and will be Andreev reflected. The reflected hole transports along the opposite direction as compared with

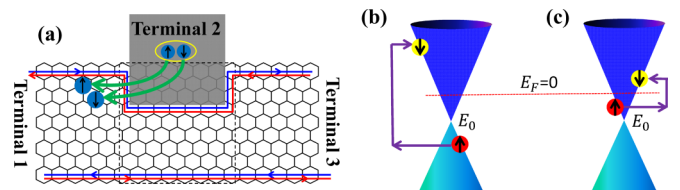


FIG. 8. (a) Schematic diagram of positive chiral edge states (red lines) for the conduction band and negative chiral edge states (blue lines) for the valence band in the three-terminal graphene/superconductor system. (b),(c) Schematic view of the specular reflection and the retroreflection in the energy space. While in the presence of the magnetic field and the chiral edge states, the specular reflection and the retroreflection are changed into the LAR and the CAR, respectively.

the incident electron. As a result, T_{11A} is considerably large and $T_{31A} = 0$ [see Figs. 7(a) and 7(c)]. In this case, the two electrons in the Cooper pair get into the same terminal [see Fig. 8(a)]. When the incident energy ω is above E_0 , the electron goes along the bottom edge state from left to right and does not encounter the superconductor. Then $T_{11A} = T_{31A} = 0$ and $T_{31N} = 1$, as shown in Figs. 7(a), 7(c), and 7(e). Similar results can be obtained for the incident electron from terminal 3. When $\omega < E_0$, the electron goes along the bottom edge state from right to left without meeting the superconductor, and $T_{13A} = T_{33A} = 0$ and $T_{13N} = 1$ [see Figs. 7(b), 7(d), and 7(f)]. When $E_0 < \omega < -E_0$ [see Fig. 8(c)], both the incident electron and the reflected hole are in the conduction band and go along the top edge states from right to left. This corresponds to the exclusive CAR process and T_{13A} has large value with $T_{33A} = 0$ [see Figs. 7(b) and 7(d)]. When $-E_0 < \omega$, the incident electron and the reflected hole are in different bands, and only the LAR happens in the graphene/superconductor interface. Note that in Figs. 7(a)–7(d), the LAR and the CAR can be separated completely by tuning the bias. Therefore, this provides us a good way to control and investigate these processes.

V. CONCLUSION

In summary, we investigate the electron transport in a three-terminal graphene/superconductor hybrid system. In high magnetic field, an exclusive crossed Andreev reflection is obtained with the aid of the edge states in the quantum Hall regime, with the other Andreev reflections being prohibited. This exclusive crossed Andreev reflection can hold by varying the size of the system and the coupling strength between the graphene and the superconductor. In particular, it can also work well for a large width of the central superconductor and is very robust against the disorder. As a result, a robust Cooper-pair splitter with high efficiency is proposed in this study. Finally, a two-dimensional electron gas/superconductor quantum Hall system is also considered, where similar results are obtained due to the chiral edge states in the system.

ACKNOWLEDGMENTS

We gratefully acknowledge the financial support from NBRP of China (Grants No. 2012CB921303 and No. 2015CB921102), NSF-China under Grants No. 11274364, No. 11504066, and No. 11574007, and FRFCU under Grant No. AUGA5710013615. Y.X. is supported by the grant of Trans-Century Training Programme Foundation for the Talents by the NCET-13-0048.

APPENDIX

In this appendix, we provide the electron transport properties of a three-terminal system, which is composed of a 2D electron gas nanoribbon and a superconductor lead [see Fig. 1(b)]. In the tight-binding representation, the Hamiltonian of the 2D electron gas nanoribbon is

$$H_{\text{HEG}} = \sum_{i,\sigma} E_i a_{i\sigma}^\dagger a_{i\sigma} - \sum_{(ij),\sigma} t e^{i\phi_{ij}} a_{i\sigma}^\dagger a_{j\sigma}. \quad (\text{A1})$$

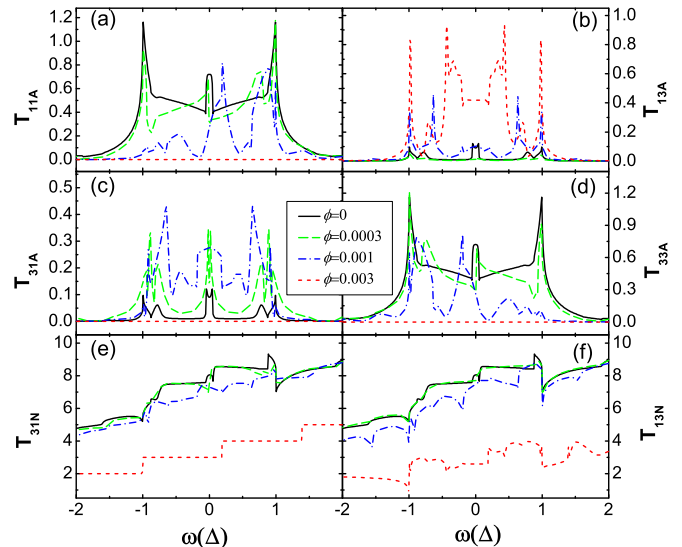


FIG. 9. Andreev reflection coefficients T_A and normal transmission coefficients T_N versus incident energy ω for a 2D electron gas/superconductor system under different magnetic fields. The parameters are $E_b = -0.02t$, $N = 100$, $L = 50$, $M = 20$, $t_c = 0.03t$, and $W = 0$.

Here $t = \frac{\hbar^2}{2ma^2}$ is the kinetic energy, $E_i = E_b + 4t + w_i$ with E_b the bottom of the conduction band, and the magnetic field is described by the magnetic flux ϕ in a square lattice. The Hamiltonians of the superconductor and the coupling between the superconductor and the electron gas are the same as Eqs. (3) and (4), respectively. Then the Andreev reflection coefficients T_A and the normal transmission coefficients T_N can be calculated from Eqs. (5) and (6). In the numerical calculation, we set the superconductor gap $\Delta = t/200$, the

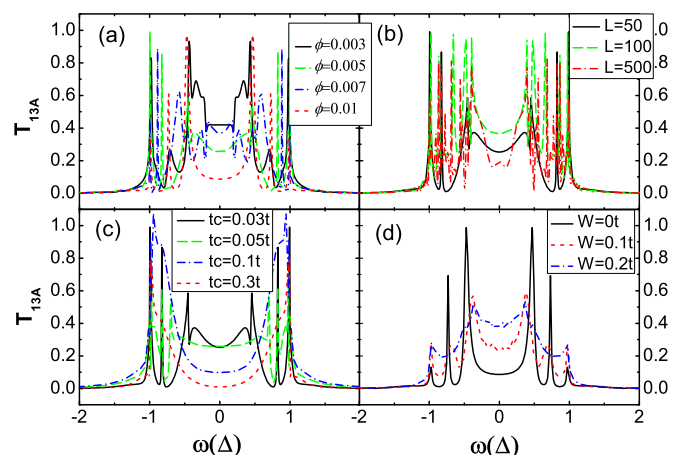


FIG. 10. T_{13A} versus ω for different ϕ (a), L (b), t_c (c), and W (d) in the electron gas/superconductor hybrid system, with $E_b = -0.02t$, $N = 100$, and $M = 20$. The other parameters are (a) $L = 50$, $t_c = 0.03t$, and $W = 0$; (b) $t_c = 0.03t$, $\phi = 0.005$, and $W = 0$; (c) $L = 50$, $\phi = 0.005$, and $W = 0$; and (d) $L = 50$, $t_c = 0.03t$, and $\phi = 0.01$. T_{11A} , T_{31A} , and T_{33A} are almost zero, so they are not shown in the figure.

conduction band bottom $E_b = -0.02t$, and the Fermi energy of the superconductor $E_F = 0$.

Figure 9 shows the transport properties under different magnetic fields. In zero or weak magnetic field, both the LAR process and the CAR one occur [see Figs. 9(a)–9(d)]. By increasing the magnetic field to $\phi = 0.003$, the edge states gradually form just as the graphene-based hybrid system. Since $\phi = a^2 B / \phi_0$, the corresponding magnetic field B is about 0.078 T for $\phi = 0.003$ and $a = 5$ nm. Due to the edge states, an exclusive CAR T_{13A} can be obtained, with the other Andreev reflection coefficients T_{11A} , T_{31A} , and T_{33A} being zero [see Figs. 9(a)–9(d)]. In addition, some Hall plateaus emerge in the curve of T_{31N} [see Fig. 9(e)], where the plateau values are determined by the filling factor ν of the Landau levels. This indicates that the incident electron from terminal 1 tunnels directly into terminal 3 without the interface scattering. With the aid of the edge states, these results can also be well understood. Now both the incident electron and the reflected hole are in the conduction band and move anticlockwise along the edge of the electron gas under high magnetic field, as shown in Fig. 1(b). For the incident electron from terminal 3, both the CAR T_{13A} and the direct tunneling T_{13N} occur. For the incident electron from terminal 1, only the direct tunneling

T_{31N} occurs. The LAR is completely prohibited, regardless of the terminal where the electron is injected. Therefore, the Cooper-pair splitter is also very efficient in the 2D electron gas/superconductor system. In fact, as long as the edge states form, one can always demonstrate a robust Cooper-pair splitter in such quantum Hall systems.

Finally, we study the exclusive CAR coefficient T_{13A} by considering the influence of the magnetic field ϕ , the length L of the central region, and the coupling strength t_c between the superconductor and the electron gas. Figures 10(a)–10(c) show T_{13A} under large magnetic field, where the Hall edge states emerge in the system. It can be seen that T_{13A} is quite large for a wide range of the system parameters, and the other Andreev reflection coefficients T_{11A} , T_{31A} , and T_{33A} are almost zero. Thus, the proposed Cooper-pair splitter based on the quantum Hall chiral edge states can work well for the large width of the central superconductor and for a wide range of the system parameters. We also consider the situation when the on-site energy disorder is introduced in the central region, as illustrated in Fig. 10(d). It is evident that T_{13A} is very robust against the disorder. These results are similar to the case of the graphene/superconductor system.

-
- [1] A. Einstein, B. Podolsky, and N. Rosen, *Phys. Rev.* **47**, 777 (1935).
- [2] M. D. Reid, P. D. Drummond, W. P. Bowen, E. G. Cavalcanti, P. K. Lam, H. A. Bachor, U. L. Andersen, and G. Leuchs, *Rev. Mod. Phys.* **81**, 1727 (2009).
- [3] J. Liu, J. Wang, and F.-C. Zhang, *Phys. Rev. B* **90**, 035307 (2014).
- [4] J. M. Byers and M. E. Flatté, *Phys. Rev. Lett.* **74**, 306 (1995).
- [5] D. Beckmann, H. B. Weber, and H.v. Löhneysen, *Phys. Rev. Lett.* **93**, 197003 (2004).
- [6] C. W. J. Beenakker, *Phys. Rev. Lett.* **97**, 067007 (2006).
- [7] J. J. He, J. Wu, T.-P. Choy, X.-J. Liu, Y. Tanaka, and K. T. Law, *Nat. Commun.* **5**, 3232 (2014).
- [8] D. Chevallier, J. Rech, T. Jonckheere, and T. Martin, *Phys. Rev. B* **83**, 125421 (2011).
- [9] P. Recher, E. V. Sukhorukov, and D. Loss, *Phys. Rev. B* **63**, 165314 (2001).
- [10] M. Veldhorst and A. Brinkman, *Phys. Rev. Lett.* **105**, 107002 (2010).
- [11] P. Recher and D. Loss, *Phys. Rev. Lett.* **91**, 267003 (2003).
- [12] P. Trocha and I. Weymann, *Phys. Rev. B* **91**, 235424 (2015).
- [13] C. Bena, S. Vishveshwara, L. Balents, and M. P. A. Fisher, *Phys. Rev. Lett.* **89**, 037901 (2002).
- [14] L. G. Herrmann, F. Portier, P. Roche, A. L. Yeyati, T. Kontos, and C. Strunk, *Phys. Rev. Lett.* **104**, 026801 (2010).
- [15] P. Recher and D. Loss, *Phys. Rev. B* **65**, 165327 (2002).
- [16] J. Wang and S. Liu, *Phys. Rev. B* **85**, 035402 (2012).
- [17] A. Schroer, P. G. Silvestrov, and P. Recher, *Phys. Rev. B* **92**, 241404(R) (2015).
- [18] Y. S. Ang, L. K. Ang, C. Zhang, and Z. Ma, *Phys. Rev. B* **93**, 041422(R) (2016).
- [19] D. S. Golubev, M. S. Kalenkov, and A. D. Zaikin, *Phys. Rev. Lett.* **103**, 067006 (2009).
- [20] M. Lee, H. Khim, and M.-S. Choi, *Phys. Rev. B* **89**, 035309 (2014).
- [21] G. B. Lesovik, T. Martin, and G. Blatter, *Eur. Phys. J. B* **24**, 287 (2001).
- [22] N. M. Chtchelkatchev, G. Blatter, G. B. Lesovik, and T. Martin, *Phys. Rev. B* **66**, 161320 (2002).
- [23] S. Russo, M. Kroug, T. M. Klapwijk, and A. F. Morpurgo, *Phys. Rev. Lett.* **95**, 027002 (2005).
- [24] L. Hofstetter, S. Csonka, J. Nygård, and C. Schönberger, *Nature (London)* **461**, 960 (2009).
- [25] L. Hofstetter, S. Csonka, A. Baumgartner, G. Fülöp, S. d’Hollosy, J. Nygård, and C. Schönberger, *Phys. Rev. Lett.* **107**, 136801 (2011).
- [26] J. Wang, L. Hao, and K. S. Chan, *Phys. Rev. B* **91**, 085415 (2015).
- [27] J. Nilsson, A. R. Akhmerov, and C. W. J. Beenakker, *Phys. Rev. Lett.* **101**, 120403 (2008).
- [28] W. Chen, R. Shen, L. Sheng, B. G. Wang, and D. Y. Xing, *Phys. Rev. B* **84**, 115420 (2011).
- [29] W. Chen, R. Shen, L. Sheng, B. G. Wang, and D. Y. Xing, *Phys. Rev. Lett.* **109**, 036802 (2012).
- [30] R. W. Reinthaler, P. Recher, and E. M. Hankiewicz, *Phys. Rev. Lett.* **110**, 226802 (2013).
- [31] Y.-T. Zhang, X. Deng, Q.-F. Sun, and Z. Qiao, *Sci. Rep.* **5**, 14892 (2015).
- [32] C.-Z. Chang, J. Zhang, X. Feng, J. Shen, Z. Zhang, M. Guo, K. Li, Y. Ou, P. Wei, L.-L. Wang, Z.-Q. Ji, Y. Feng, S. Ji, X. Chen, J. Jia, X. Dai, Z. Fang, S.-C. Zhang, K. He, Y. Wang, L. Lu, X.-C. Ma, and Q.-K. Xue, *Science* **340**, 167 (2013).
- [33] J. G. Checkelsky, R. Yoshimi, A. Tsukazaki, K. S. Takahashi, Y. Kozuka, J. Falson, M. Kawasaki, and Y. Tokura, *Nat. Phys.* **10**, 731 (2014).
- [34] C. W. J. Beenakker, *Rev. Mod. Phys.* **80**, 1337 (2008).

- [35] A. H. Castro Neto, F. Guinea, N. M. R. Peres, K. S. Novoselov, and A. K. Geim, *Rev. Mod. Phys.* **81**, 109 (2009).
- [36] H. Hoppe, U. Zülicke, and Gerd Schön, *Phys. Rev. Lett.* **84**, 1804 (2000).
- [37] N. M. Chtchelkatchev, *JETP Lett.* **73**, 94 (2001).
- [38] J. Eroms, D. Weiss, J. De Boeck, G. Borghs, and U. Zülicke, *Phys. Rev. Lett.* **95**, 107001 (2005).
- [39] P. Rickhaus, M. Weiss, Laurent Marot, and C. Schönenberger, *Nano. Lett.* **12**, 1942 (2012).
- [40] P. Carmier, *Phys. Rev. B* **88**, 165415 (2013).
- [41] D. N. Sheng, L. Sheng, and Z. Y. Weng, *Phys. Rev. B* **73**, 233406 (2006).
- [42] W. Long, Q.-F. Sun, and J. Wang, *Phys. Rev. Lett.* **101**, 166806 (2008).
- [43] J. R. Williams, L. DiCarlo, and C. M. Marcus, *Science* **317**, 638 (2007).
- [44] J.-c. Chen, T. C. Au, Yeung, and Q.-f. Sun, *Phys. Rev. B* **81**, 245417 (2010).
- [45] J. Martin, N. Akerman, G. Ulbricht, T. Lohmann, J. H. Smet, K. von Klitzing, and A. Yacoby, *Nat. Phys.* **4**, 144 (2007).
- [46] Y. Zhang, V. W. Brar, C. Girit, A. Zettl, and M. F. Crommie, *Nat. Phys.* **5**, 722 (2009).
- [47] Q.-F. Sun and X. C. Xie, *J. Phys. Condens. Matter* **21**, 344204 (2009).
- [48] Q.-F. Sun, J. Wang, and T.-H. Lin, *Phys. Rev. B* **59**, 3831 (1999).
- [49] Q.-F. Sun, J. Wang, and T.-H. Lin, *Phys. Rev. B* **59**, 13126 (1999).
- [50] D. H. Lee and J. D. Joannopoulos, *Phys. Rev. B* **23**, 4997 (1981); M. P. López Sancho, J. M. López Sancho, and J. Rubio, *J. Phys. F* **14**, 1205 (1984); **15**, 851 (1985).
- [51] R. Mélin, F. S. Bergeret, and A. Levy Yeyati, *Phys. Rev. B* **79**, 104518 (2009).
- [52] S.-G. Cheng, Y. Xing, J. Wang, and Q.-F. Sun, *Phys. Rev. Lett.* **103**, 167003 (2009).
- [53] G. E. Blonder, M. Tinkham, and T. M. Klapwijk, *Phys. Rev. B* **25**, 4515 (1982); G. Deutscher, *Rev. Mod. Phys.* **77**, 109 (2005).
- [54] J. Cayssol, *Phys. Rev. Lett.* **100**, 147001 (2008).
- [55] J. Linder, M. Zareyan, and A. Sudbø, *Phys. Rev. B* **80**, 014513 (2009).
- [56] Y. Xing, J. Wang, and Q.-F. Sun, *Phys. Rev. B* **83**, 205418 (2011).